Article

Impact of Annealing Temperature on the Morphological, Optical and Photoelectrochemical Properties of Cauliflower-like CdSe$_{0.6}$Te$_{0.4}$ Photoelectrodes; Enhanced Solar Cell Performance

Gajanan S. Ghodake [1] [ID], Dae-Young Kim [1], Surendra K. Shinde [1,*], Deepak P. Dubal [2], Hemraj M. Yadav [1] and Verjesh Kumar Magotra [3] [ID]

[1] Department of Biological and Environmental Science, College of Life Science and Biotechnology, Dongguk University, 32 Dongguk-ro, Biomedical Campus, Ilsandong-gu, Siksa-dong, Goyang-si 10326, Korea; ghodakegs@gmail.com (G.S.G.); sbpkim@dongguk.edu (D.-Y.K.); hemrajy@gmail.com (H.M.Y.)
[2] School of Chemistry and Physics, Queensland University of Technology (QUT), 2 George Street, Brisbane, QLD 4001, Australia; deepak.dubal@qut.edu.au
[3] Nano Information Technology Academy, Dongguk University, Seoul 100715, Korea; birju.srm@gmail.com
* Correspondence: surendrashinde@dongguk.edu; Tel./Fax: +82-31-961-5122

Abstract: We are reporting on the impact of air annealing temperatures on the physicochemical properties of electrochemically synthesized cadmium selenium telluride (CdSe$_{0.6}$Te$_{0.4}$) samples for their application in a photoelectrochemical (PEC) solar cell. The CdSe$_{0.6}$Te$_{0.4}$ samples were characterized with several sophisticated techniques to understand their characteristic properties. The XRD results presented the pure phase formation of the ternary CdSe$_{0.6}$Te$_{0.4}$ nanocompound with a hexagonal crystal structure, indicating that the annealing temperature influences the XRD peak intensity. The XPS study confirmed the existence of Cd, Se, and Te elements, indicating the formation of ternary CdSe$_{0.6}$Te$_{0.4}$ compounds. The FE-SEM results showed that the morphological engineering of the CdSe$_{0.6}$Te$_{0.4}$ samples can be achieved simply by changing the annealing temperatures from 300 to 400 °C with intervals of 50 °C. The efficiencies (η) of the CdSe$_{0.6}$Te$_{0.4}$ photoelectrodes were found to be 2.0% for the non-annealed and 3.1, 3.6, and 2.5% for the annealed at 300, 350, and 400 °C, respectively. Most interestingly, the PEC cell analysis indicated that the annealing temperatures played an important role in boosting the performance of the photoelectrochemical properties of the solar cells.

Keywords: electrodeposition; CdSe$_{0.6}$Te$_{0.4}$; thin films; XRD; EDS; DSSC; solar cell

1. Introduction

With the rapid increase in the world's population and environmental pollution, there is limited availability of energy sources. A worldwide demand therefore exists for new energy sources that are clean, cost-effective, and simple and that do not cause environmental pollution [1,2]. Various energy storage devices available on the electronic markets include fuel cells [3], solar cells [4,5], H$_2$ evolution systems [6,7], light-emitting diodes (LED) [8], capacitors [9], supercapacitors [10,11], and batteries [12]. Among these, the photoelectrochemical (PEC) cell is the best electronic device because of the easy and whole-day availability of sunlight on Earth, whereas the convenience of the other sources of materials is geographically limited. To improve the electrical properties of its solar cells, the PEC has two main principal requirements, which are related to the band gap energy and the stability of the photoelectrodes. First, the photoelectrode should provide the band gap of materials whose band gap energy is nearly matched to the extreme sunlight intensity in the visible spectrum to use the solar spectrum resourcefully (1–3 eV). Second, the semiconductor photoelectrode materials need to be stable with respect to the 1 M polysulfide (NaOH:Na$_2$S:S) liquid electrolytes during the PEC measurements.

To date, several binary metal chalcogenide photoelectrode materials have been developed into PECs as photoabsorber layers, including CdS [13,14], CdSe [15,16], CdTe [17], ZnS [18], ZnSe [19], and ZnSe/CdSe [20]. Among these binary photoelectrode materials, CdSe and CdTe materials provided band gap values between 1.45 and 1.75 eV [1,21–30]; this indicates that the lower band gap energy photoelectrodes provided higher optical absorption. The higher optical absorption of the photoelectrode material provides more electron–hole pairs as well as a higher rate of the recombination rates of charge carriers [21,22]. The significance of selecting particular compositions is that the $CdSe_{0.6}Te_{0.4}$ electrode shows a sharp transition from the properties of CdSe to those typical of CdTe in the composition [31]. The second reason for the selection of the ternary $CdSe_{0.6}Te_{0.4}$ compounds is to improve the electrical and optical properties of the binary CdSe and CdTe metal chalcogenides. Recently, various co-workers have been working on the $CdSe_XTe_{1-X}$ compounds and finally concluded that the $CdSe_{0.6}Te_{0.4}$ composition shows better photoelectrochemical properties than the other composition/photoelectrodes [23–31].

Currently, researchers have been using various chemical and physical deposition methods, such as molecular beam epitaxy (MBE) [23,24], chemical vapor [25], hydrothermal [26], radiofrequency sputtering [27], slurry coating [28], non-injection one-pot [29], silicon isolation layer [30], electrodeposition [31], and chemical bath deposition (CBD) [32], to develop ternary $CdSe_{0.6}Te_{0.4}$ thin films for various applications. Among these methods, the electrodeposition method is simple, rapid, and scalable for preparing ternary $CdSe_{0.6}Te_{0.4}$ samples [31–37]. Our previous study investigated the deposition of ternary $CdSe_{0.6}Te_{0.4}$ composites under different conditions, such as varying bath concentrations, deposition times, and electron-beam irradiation doses [31–37]. However, to the best of our knowledge, the effect of the annealing temperature at different temperature intervals of 50 °C on the morphological engineering of the ternary $CdSe_{0.6}Te_{0.4}$ composites for PEC has not been reported.

In this work, we present the effect of different annealing temperatures on the structural, morphological, and photoelectrical properties of as-deposited $CdSe_{0.6}Te_{0.4}$ composites. As-fabricated $CdSe_{0.6}Te_{0.4}$ composites were subsequently characterized using physical techniques such as a structural analysis by XRD, compositional and elemental analyses by XPS and EDS, surface morphology observations by FE-SEM, and *J-V* measurements to evaluate their PEC properties. After the air annealing treatment, the $CdSe_{0.6}Te_{0.4}$ samples showed improvements in their structural, morphological, and photoelectrical properties. A maximum power efficiency (η) of 3.6% for the $CdSe_{0.6}Te_{0.4}$ photoelectrode was realized when the sample was annealed at 350 °C at a 30 mV cm^{-2} power input in a 1 M polysulfide electrolyte. The FE-SEM results of the $CdSe_{0.6}Te_{0.4}$ samples show that variations in the annealing temperature result in different surface morphologies, which range from cauliflower-like to broccoli-like to coral-like nanostructures.

2. Results and Discussion

2.1. X-ray Diffraction

The non-annealed and annealed $CdSe_{0.6}Te_{0.4}$ composites were studied by XRD to identify their phase formation and crystal structures. Figure 1a shows the XRD patterns of the non-annealed $CdSe_{0.6}Te_{0.4}$ composites and the annealed at different temperatures. The peaks in the patterns obtained for all the ternary $CdSe_{0.6}Te_{0.4}$ composites are well matched to the standard JCPDS card number 41–1325. The peaks at 24.09°, 25.16°, 27.63°, 38.53°, 40.26°, 42.01°, 44.51°, 49.91°, 57.02°, and 63.69° correspond to the (100), (002), (101), (102), (110), (111), (103) (201), (202), and (203) diffraction planes, respectively, confirming the polycrystalline hexagonal crystal structure of both $CdSe_{0.6}Te_{0.4}$ samples [35–37]. After the annealing treatments, the XRD patterns of the $CdSe_{0.6}Te_{0.4}$ samples show increased sharpness and higher peak intensity as compared to the non-annealed samples. We clearly observed the $CdSe_{0.6}Te_{0.4}$ samples annealed at 350 °C, and the samples showed enhanced peak intensity and sharpness compared to all the $CdSe_{0.6}Te_{0.4}$ samples [38,39]. However, in the $CdSe_{0.6}Te_{0.4}$ samples annealed at the higher temperature of 400 °C, the XRD patterns

show that the peak intensity decreases, confirming that the annealing temperature affects the crystallinity and peak sharpness of the $CdSe_{0.6}Te_{0.4}$ samples. The XRD results indicate the formation of the pure phase of the ternary $CdSe_{0.6}Te_{0.4}$ composites without any other impurities such as binary CdSe and CdTe nanomaterial. Su et al. [40] reported on CdSeTe quantum dots with a cubic crystal structure prepared via an aqueous solution method and their suitability for use in PECs and water-splitting applications; they concluded that the as-prepared CdSeTe quantum dots were useful for enhancing the photo power efficiency and stability of the solar cells. MacDonald et al. [41] explored the band gap energy and electrical properties of $CdSe_xTe_{1-x}$ nanocrystals with various CdSe and CdTe contents. We calculated the crystallite size of the non-annealed and annealed $CdSe_{0.6}Te_{0.4}$ samples at their greatest peak intensity (101) of the XRD patterns using standard Scherrer's formula. The calculated crystallite size of the non-annealed samples was 36 nm; after annealing at 300, 350, and 400 °C, the crystallite sizes of the $CdSe_{0.6}Te_{0.4}$ samples were 27, 16, and 23 nm, respectively. The decrease in crystallite size from 36 to 16 nm can be attributed to the recrystallization of the $CdSe_{0.6}Te_{0.4}$ thin films at various temperatures. The obtained values of the crystallite sizes show that when annealed at a temperature of 350 °C, the crystallite size is smaller than the other samples, and this size contraction is attributable to the heat treatment [37].
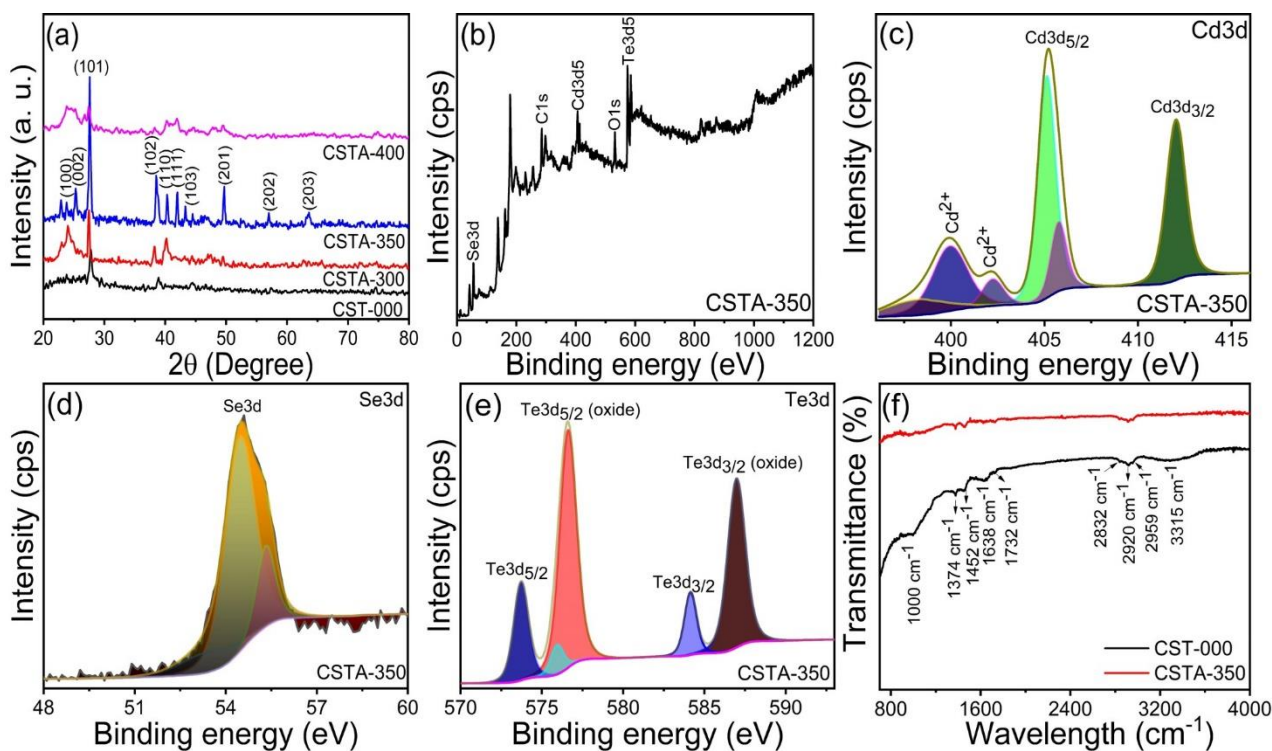
Figure 1. (**a**) XRD patterns of the non-annealed and annealed $CdSe_{0.6}Te_{0.4}$ thin films at various temperatures; (**b**) survey spectra of optimized $CdSe_{0.6}Te_{0.4}$ thin films, (**c**–**e**) core levels of Cd, Se, and Te of the optimized $CdSe_{0.6}Te_{0.4}$ thin films, respectively; (**f**) FT-IR spectra of non-annealed and optimized annealing temperature at 350 °C of the $CdSe_{0.6}Te_{0.4}$ thin films, respectively.

2.2. X-ray Photoelectron Spectroscopy

Figure S1 and Figure 1b show the survey spectra of the non-annealed $CdSe_{0.6}Te_{0.4}$ samples and the annealed at 350 °C to determine their elemental compositions and chemical valence states. Both spectra of samples show peaks associated with Cd 3d, Se 3d, C 1s, O 1s, and Te 3d elements, indicating the successful formation of ternary $CdSe_{0.6}Te_{0.4}$ thin films. Figure 1c–e shows the core-level spectra of Cd 3d, Se 3d, and Te 3d, respectively. As shown in Figure 1c, the major characteristic peaks at binding energies of 405.26 and 411.99 eV correspond to the Cd $3d_{5/2}$ and Cd $3d_{3/2}$ states, respectively [34]. The difference between

the binding energies is approximately 6.73 eV, which is consistent with the formation of the ternary $CdSe_{0.6}Te_{0.4}$ compound [38]. The peaks observed at the binding energy of 400 eV, which is related to the surface of the Cd^{2+} ions, formed on the surface of the $CdSe_{0.6}Te_{0.4}$ samples [6,39,40]. The peak observed at 54.55 eV corresponds to the Se 3d region shown in Figure 1d, which indicates that the Se element is present in $CdSe_{0.6}Te_{0.4}$ sample. Figure 1e shows the Te 3d spectral region of the $CdSe_{0.6}Te_{0.4}$ sample annealed at a temperature of 350 °C. The spectra of the Te 3d show characteristic peaks at binding energies of 573.75 and 584.20 eV, which correspond to the Te $3d_{5/2}$ and Te $3d_{3/2}$ states, respectively (shown in Figure 1e) [4,40,41]. The Te 3d core-level spectra show the two other peaks observed at binding energies of 576.66 and 586.96 eV, which are assigned to Te $3d_{5/2}$ oxide and Te $3d_{3/2}$ oxide, respectively [42]. The XPS survey spectrum of both $CdSe_{0.6}Te_{0.4}$ samples shows the two other peaks at the binding energies of 284.56 and 531.56 for the C ls and O 1s peaks, respectively. The carbon peaks observed on the surface of the samples may be due to the carbon tape used for the preparation of the XPS analysis. The O 1s peaks can be attributed to the samples prepared in an aqueous solution and annealing in air atmospheric conditions. Thus, the XPS results confirm that Cd, Se, and Te elements are present in the $CdSe_{0.6}Te_{0.4}$ sample both before and after annealing, which indicates the formation of the $CdSe_{0.6}Te_{0.4}$ compound [43].

2.3. FT-IR

Figure 1f shows the FT-IR spectra of the non-annealed $CdSe_{0.6}Te_{0.4}$ and of the sample annealed at 350 °C to determine their vibrational characteristics. As shown in Figure 1f, the FT-IR spectrum of the non-annealed sample shows a broad characteristic peak at 3315 cm^{-1}, which is related to the surface hydroxide (O–H) groups because of the adsorbed water in the non-annealed $CdSe_{0.6}Te_{0.4}$. In the spectrum of the annealed sample, the O–H peak disappeared because the water was volatilized during annealing at 350 °C. In Figure 1f, the characteristic peaks at 2832, 2920, and 2959 cm^{-1} in the spectra of both $CdSe_{0.6}Te_{0.4}$ samples correspond to CH_2–S bonding [40]. Peaks related to the asymmetric vibrational mode of the C–O bonds are observed at 1732 and 1638 cm^{-1} in the spectra of both the samples. These two peaks confirm the presence of L-cys on $CdSe_{0.6}Te_{0.4}$ [44]. The spectra of both the non-annealed and annealed $CdSe_{0.6}Te_{0.4}$ samples show a vibrational peak at 1452 cm^{-1}, which is related to the symmetric stretching vibration of the C–N bonds [45,46]. The stronger peaks in the range of 1000–1374 cm^{-1} correspond to a Cd-Se-Te composite formed in both the non-annealed and annealed $CdSe_{0.6}Te_{0.4}$ samples. The FT-IR spectra confirm the formation of pure-phase $CdSe_{0.6}Te_{0.4}$ thin films.

2.4. FE-SEM

FE-SEM analyses were used to study the surface morphology of the non-annealed $CdSe_{0.6}Te_{0.4}$ samples as well as the effect of the annealing on their surface morphology. Figure 2a–h presents the FE-SEM analyses of the non-annealed $CdSe_{0.6}Te_{0.4}$ samples and those annealed at different temperatures (300, 350, and 400 °C) with different magnifications. All the samples are fully covered with uniform thin films of various nanostructures with cauliflower-like, broccoli-like, and coral-like morphologies with various temperatures. Figure 2a,b presents the FE-SEM images of the non-annealed $CdSe_{0.6}Te_{0.4}$ samples at different magnifications. At higher magnifications, cauliflower-like nanostructures are clearly observed to fully cover the surface of the samples [32–34]. The FE-SEM images of the $CdSe_{0.6}Te_{0.4}$ samples annealed in air exhibit various surface morphologies, as shown in Figure 2c–h. The surface of the $CdSe_{0.6}Te_{0.4}$ sample annealed at 300 °C exhibits vertical nanorod-like nanostructures. Further, the growth of nanoleaves is clearly observed at the top of the nanorods, possibly because of the annealing treatment [47–49]. These results suggest that annealing is useful for developing various surface structures.
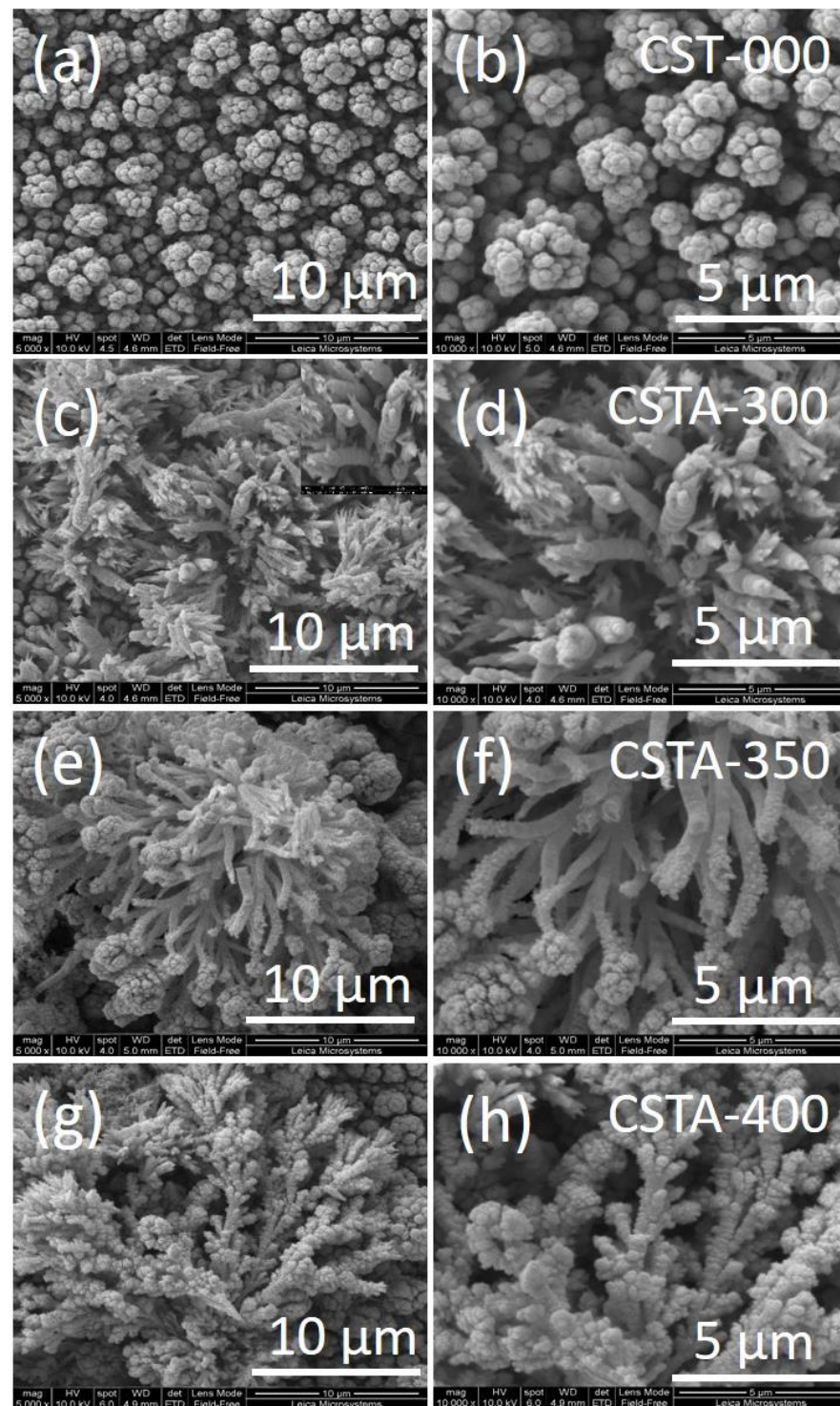
Figure 2. FE-SEM images of the CdSe$_{0.6}$Te$_{0.4}$ thin films non-annealed using the (**a,b**) electrochemical method, at air annealing temperatures of (**c,d**) 300 °C, (**e,f**) 350 °C, and (**g,h**) 400 °C. Scale bars in (**a,c,e,g**): 10 μm; (**b,d,f,h**): 5 μm.

When we increased the annealing temperature from 300 to 350 °C, the treated CdSe$_{0.6}$Te$_{0.4}$ sample exhibited a unique, porous morphology, as shown in Figure 2e,f. The images clearly show that the surface is highly porous and that one end of the tubes is open, which is useful for PEC applications. The image of the other end shows flower-bouquet-like morphology developed on the nanotubes. Similar morphology has been reported to strongly influence PEC performance because these types of morphology provide a larger surface area [33].

Further, when the annealing temperature increased to 400 °C, samples with tree-branch-like morphology were observed, as shown in Figure 2g,h. The surface morphological studies confirmed that the annealing temperature affected the porosities, morphology, and active surface areas of the $CdSe_{0.6}Te_{0.4}$ sample [34,50]. The schematic formation and effect of the annealing temperature on the $CdSe_{0.6}Te_{0.4}$ nanostructures are presented in Scheme 1.
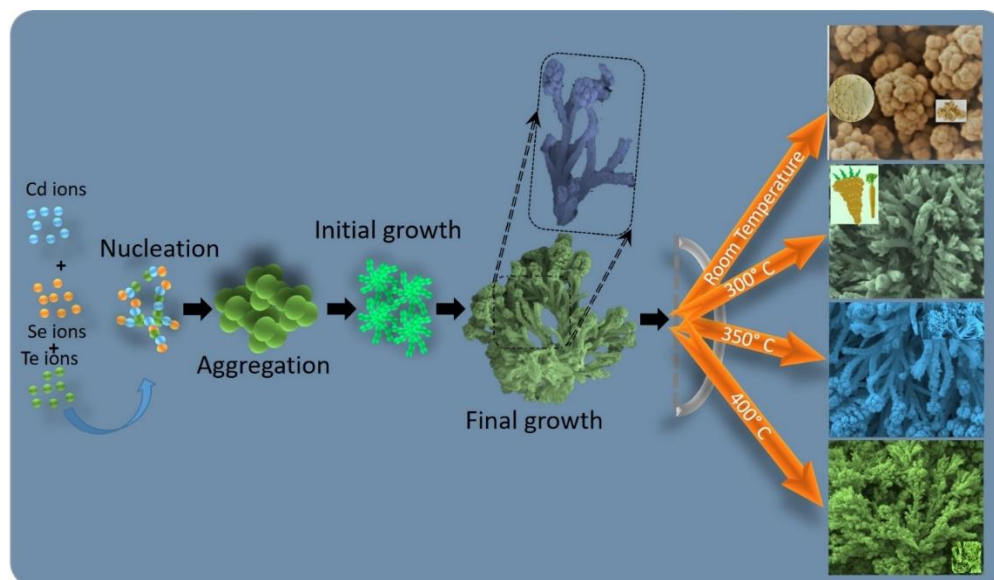
Scheme 1. Schematic formation and effect of air annealing temperature on the $CdSe_{0.6}Te_{0.4}$ nanostructures.

Figure 3a–h shows the EDS spectra and elemental mapping images of the non-annealed $CdSe_{0.6}Te_{0.4}$ and the air-annealed sample at 350 °C, respectively. The EDS analysis showed that Cd, Se, and Te elements are present in both the non-annealed and optimized $CdSe_{0.6}Te_{0.4}$ samples. The EDS analysis also revealed the presence of O in both the samples because all the samples were prepared in water; the XPS results supported the EDS analysis. Moreover, Pt was observed because a Pt coating was applied to the samples for the FE-SEM analysis [34–37].
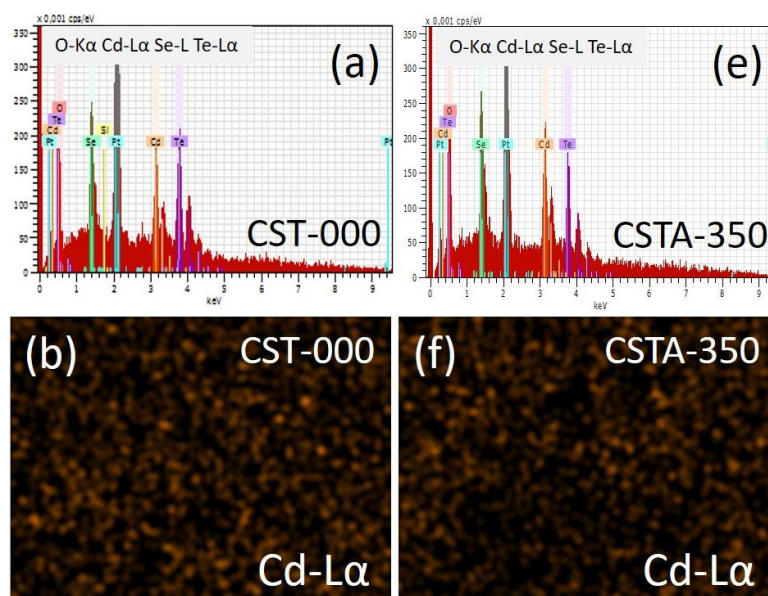
Figure 3. *Cont.*
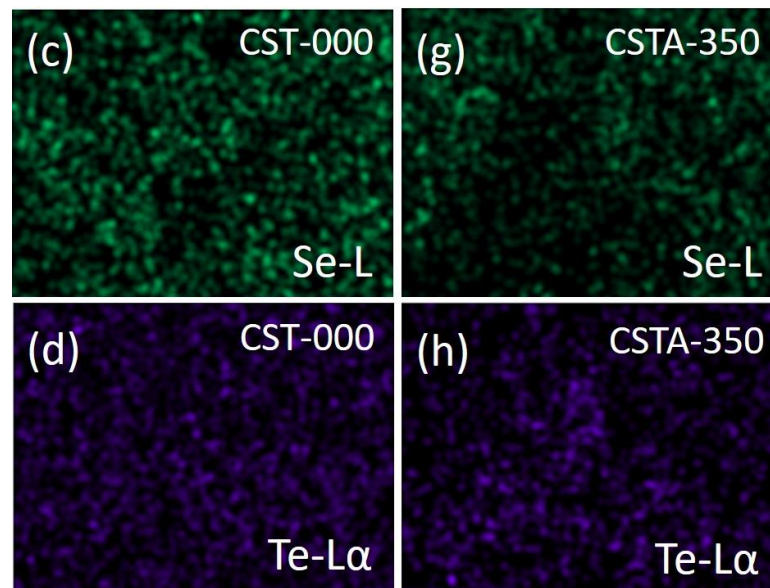
Figure 3. (**a–h**) EDS and elemental mapping of non-annealed and optimized annealing temperature at 350 °C of CdSe$_{0.6}$Te$_{0.4}$, respectively.

2.5. Band Gap Energy Study

Figure 4 shows the optical band gap energy plots of the non-annealed CdSe$_{0.6}$Te$_{0.4}$ samples and the annealed ones at 300, 350, and 400 °C. The optical band gap energy was obtained using the following Equation (1) [35]:

$$\alpha = \frac{A(h\nu - E_g)^{n/2}}{h\nu} \tag{1}$$

where A and n are constants, "hν" is the photon energy, and E$_g$ is the band gap energy. The direct and indirect band gap energies of semiconductor materials depend on the aforementioned values. The band gap energy results indicate that the non-annealed and annealed CdSe$_{0.6}$Te$_{0.4}$ samples are semiconductor materials with direct band gap energies.
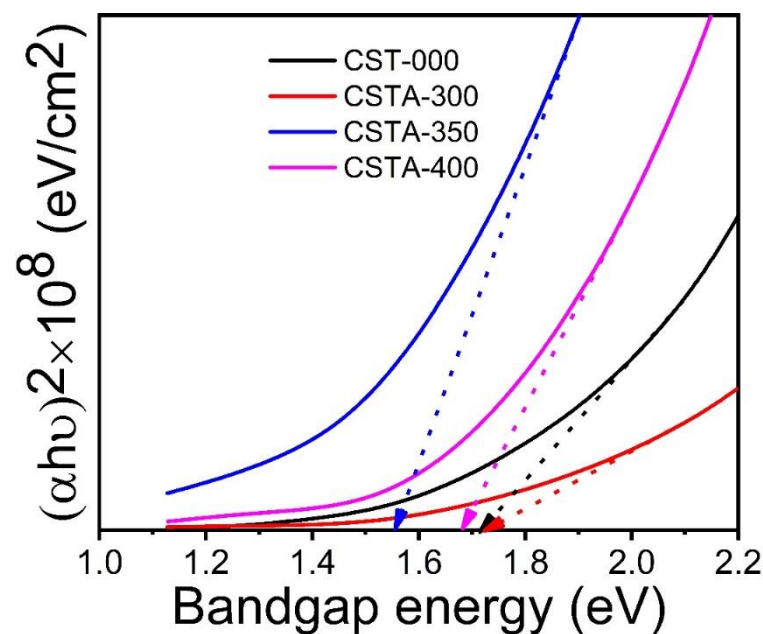
Figure 4. Band gap energy curves of the non-annealed and annealing temperatures of CdSe$_{0.6}$Te$_{0.4}$ samples.

The E_g value of the non-annealed $CdSe_{0.6}Te_{0.4}$ samples was 1.70 eV; after annealing the $CdSe_{0.6}Te_{0.4}$ samples at 300 °C, the band gap energy slightly increased to 1.72 eV. Furthermore, by increasing the annealing temperature from 300 to 350 °C, the band gap energy decreased to 1.55 eV. The optical band gap energy value decreased with increasing air annealing temperature; this change is attributable to the changes in the nanostructures and thermal defects of the $CdSe_{0.6}Te_{0.4}$ thin films. However, when we studied the effect of the higher temperature on $CdSe_{0.6}Te_{0.4}$ thin films at 400 °C, the band gap energy increased up to 1.69 eV. The version of the band gap energy values demonstrated that redshift occurs in all the $CdSe_{0.6}Te_{0.4}$ thin films [21,51,52]. Muthukumarasamy et al. [53] prepared the $CdSe_xTe_{1-x}$ ternary composite on conducting glass substrates using the hot-wall deposition method with a varying composition of Se and Te precursors (x = 0.15, 0.4, 0.6, 0.7, 0.85). They reported that band gap energies increased in the range from 1.54 to 1.72 eV. Velumani et al. [54] reported that band gap energies increased between 1.52 and 1.62 eV, and Sathyamoorthy et al. [55] reported band gap energies in the ranges of 1.52 to 2.66 eV. These reported values of the band gap energies are in good agreement with the reported values in the present work.

2.6. Photoelectrochemical Study

Figure 5 shows the *J-V* measurement curves for the non-annealed and the annealed $CdSe_{0.6}Te_{0.4}$ photoelectrodes at different temperatures in the range from 300 to 400 °C, respectively. The photocurrent density of the non-annealed $CdSe_{0.6}Te_{0.4}$ photoelectrode was 1.91 mA cm^2, and the photocurrent densities of the $CdSe_{0.6}Te_{0.4}$ photoelectrodes annealed at 300, 350 and 400 °C were 2.59, 2.96, and 2.15 mA cm^2, respectively. After annealing in air, the $CdSe_{0.6}Te_{0.4}$ photoelectrode showed measurable changes in the photocurrent density and minor changes in the photovoltage, where the magnitude of the changes depends on the annealing temperature of the $CdSe_{0.6}Te_{0.4}$ photoelectrode. These results suggest that the annealing temperatures influence the photocurrent density of all the annealed $CdSe_{0.6}Te_{0.4}$ photoelectrodes. The *J-V* measurement presented that the $CdSe_{0.6}Te_{0.4}$ photoelectrode annealed at 350 °C exhibits the highest photocurrent density of 2.96 mA cm^2, which is attributed to its highly porous and hollow-nanowire-like surface morphology. The fill factor (FF) was obtained by the following standard relation Equation (2) [48]:

$$FF = \frac{I_{max} \times V_{max}}{V_{oc} \times I_{sc}} \tag{2}$$
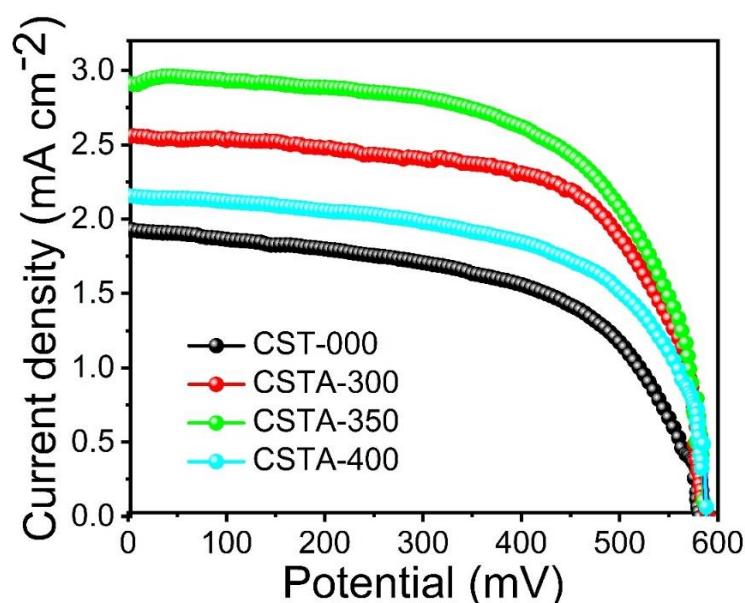
Figure 5. *J-V* curves of non-annealed $CdSe_{0.6}Te_{0.4}$ photoelectrodes and air annealing with different temperatures of 300, 350, and 400 °C.

Another significant feature of solar cells is their efficiency (η). The solar cell η is directly related to the ratio of the output power to the incident light on the working photoelectrodes. The η was obtained using the standard Equation (3) [31,33]:

$$\eta(\%) = \frac{V_{oc} \times I_{sc}}{P_{input}} \times FF \times 100 \qquad (3)$$

The values of I_{max}, V_{max}, I_{sc}, V_{oc}, FF, and η for the non-annealed and annealed CdSe$_{0.6}$Te$_{0.4}$ photoelectrodes are reported in Table 1. Table 1 presents the values of power η of the non-annealed and annealed CdSe$_{0.6}$Te$_{0.4}$ photoelectrodes as 2.0, 3.1, 3.6, and 2.5 %, respectively. The resultant values of η indicate that temperatures are positively affected on the ternary metal chalcogenides CdSe$_{0.6}$Te$_{0.4}$ photoelectrodes. The value of η increased with increasing annealing temperatures up to 350 °C and then decreased when the annealing temperature was further increased to 400 °C, which may be due to the band gap energy and porous nanostructures [35,37]. The lower band gap energy and highly porous surface morphology of photoelectrodes provided more electron–hole pairs and higher surface areas as compared to the other photoelectrodes for PEC application. The results of the η values indicate that the annealing temperature affects both the surface morphology and the solar cell performance. The CdSe$_{0.6}$Te$_{0.4}$ sample annealed at 350 °C exhibited the best solar cell performance among the investigated samples because of its highly porous, nanowire-like surface structure, which provides abundant active sites for the separation of charge carriers [30–33].

Table 1. PEC parameters like open-circuit voltage (V_{OS}), short-circuit current (I_{SC}), fill factor (FF), and efficiency (η) of as-prepared and air-annealed samples at different annealing temperatures.

Samples Names/ID	I_{max} (mA/cm^2)	V_{max} (mV/cm^2)	V_{OC} (mV/cm^2)	I_{SC} (mA/cm^2)	Fill Factor	Efficiency (η) %
CST-000	1.50	409.21	658.37	1.91	0.49	2.0
CSTA-300	2.30	407.71	671.04	2.59	0.54	3.1
CSTA-350	2.66	407.14	680.25	2.96	0.53	3.6
CSTA-400	1.83	413.13	697.29	2.19	0.50	2.5

3. Materials and Methods

3.1. Materials

The reagents used to prepare the CdTe$_{0.6}$Se$_{0.4}$ samples were 0.1 M cadmium sulfate monohydrate (CdSO$_4$·H$_2$O), 0.01 M selenium dioxide (SeO$_2$), 0.02 M sodium telluride (Na$_2$TeO$_3$), and EDTA. All the chemicals were purchased from Sigma-Aldrich (Incheon, Korea).

3.2. Synthesis of CdTe$_{0.6}$Se$_{0.4}$ Thin Films

The CdSe$_{0.6}$Te$_{0.4}$ was deposited on stainless steel (SS) and fluorine-doped tin oxide (FTO) glass by using the potentiostatic method. Precleaned SS and FTO were used as working electrodes while SCE and graphite served as reference and counter electrode, respectively. The dried substrates with an area of 1 cm^2 were immersed in an electrolyte solution containing CdSO$_4$·8H$_2$O, SeO$_2$, Na$_2$TeO$_3$, and EDTA to deposit the CdSe$_{0.6}$Te$_{0.4}$. After 30 min, the substrates were removed and cleaned using DDW. The non-annealed and annealed samples at 300, 350, and 400 °C are denoted as CST-000, CSTA-300, CSTA-350, and CSTA-400, respectively [33,37].

3.3. Characterization Techniques

A Philips PW-3710 X-ray powder diffractometer (λ = 1.54 Å, Cu-K$_\alpha$) was used to measure the structural properties of the samples in the range of 20–80°. FE-SEM was then conducted using a JEOL JSM-6360 to observe the surface morphologies of all samples. The optical properties of the composite samples deposited on the FTO substrates were studied

using a Systronics model 119 spectrophotometer. The XPS analysis was performed using a Physical Electronics 5600 Multi-technique system equipped with a monochromatic Al K_α radiation source to analyze the surface compositions of the samples [36,37].

3.4. Electrode Preparation and PEC Measurements

The PECs were fabricated in a two-electrode configuration comprising n-CdSe$_{0.6}$Te$_{0.4}$ composites as a photoanode and graphite as a counter electrode; 1 M polysulfide (NaOH:Na$_2$S:S) was used as the redox electrolyte. The PEC cell was illuminated with a 100 W tungsten-filament lamp (I = 30 mW cm^{-2}) to measure the short-circuit current (I$_{sc}$) and open-circuit voltage (V$_{oc}$).

4. Conclusions

Here, we systematically investigated the effect of different annealing temperatures on CdSe$_{0.6}$Te$_{0.4}$ composite samples for use in PEC cells. All the non-annealed and annealed samples were polycrystalline in nature with a hexagonal structure. The FE-SEM analysis showed that the surface morphologies can be altered by the annealing temperature. The surface morphologies such as cauliflower-like, broccoli-like, and coral-like structures were developed on the surface of the substrate. The optical band gap of the CdSe$_{0.6}$Te$_{0.4}$ samples was in the range of 1.70–1.55 eV, suggesting that the ternary CdSe$_{0.6}$Te$_{0.4}$ composite is suitable for use in PEC solar cells. The maximum η and FF of this PEC cell were 3.6 % and 0.53, respectively, as observed for the photoelctrode annealed at 350 °C.

Supplementary Materials: The following are available online at https://www.mdpi.com/article/10.3390/ijms222111610/s1.

Author Contributions: Conceptualization, S.K.S. and D.-Y.K.; methodology, S.K.S. and H.M.Y.; software, S.K.S.; validation, V.K.M. and D.P.D.; formal analysis, S.K.S. and D.-Y.K.; investigation, D.P.D.; resources, D.-Y.K.; data curation, S.K.S.; writing—original draft preparation, S.K.S.; writing—review and editing, S.K.S. and D.-Y.K.; visualization, S.K.S., and D.-Y.K.; supervision, S.K.S., D.-Y.K. and G.S.G. All authors have read and agreed to the published version of the manuscript.

Data Availability Statement: The data presented in this study are available on request from the corresponding author. The data are not publicly available due to privacy. Data is contained within the article or Supplementary Materials.

Conflicts of Interest: The authors declare no conflict of interest.

References

1. Chang, H.; Wu, H. Graphene-based nanocomposites: Preparation, functionalization, and energy and environmental applications. *Energy Environ. Sci.* **2013**, *6*, 3483–3507. [CrossRef]
2. Sun, M.-H.; Huang, S.-Z.; Chen, L.-H.; Li, Y.; Yang, X.-Y.; Yuan, Z.-Y.; Su, B.-L. Applications of hierarchically structured porous materials from energy storage and conversion, catalysis, photocatalysis, adsorption, separation, and sensing to biomedicine. *Chem. Soc. Rev.* **2016**, *45*, 3479–3563. [CrossRef]
3. Antoniadou, M.; Kondarides, D.I.; Dionysiou, D.D.; Lianos, P. Quantum dot sensitized titania applicable as photoanode in photoactivated fuel cells. *J. Phys. Chem. C* **2012**, *116*, 16901–16909. [CrossRef]
4. De, B.; Karak, N. Recent progress in carbon dot–metal based nanohybrids for photochemical and electrochemical applications. *J. Mater. Chem. A* **2017**, *5*, 1826–1859. [CrossRef]
5. Yang, J.; Wang, J.; Zhao, K.; Izuishi, T.; Li, Y.; Shen, Q.; Zhong, X. CdSeTe/CdS Type-I Core/Shell Quantum Dot Sensitized Solar Cells with Efficiency over 9%. *J. Phys. Chem. C* **2015**, *119*, 28800–28808. [CrossRef]
6. Su, X.; Chen, Y.; Ren, L.; He, Y.; Yin, X.; Liu, Y.; Yang, W. Cobalt catalyst grafted CdSeTe quantum dots on porous NiO as photocathode for H2 evolution under visible light. *ACS Sustain. Chem. Eng.* **2019**, *7*, 11166–11174. [CrossRef]
7. Zhang, Y.; Yin, P.F.; Liu, X.; Mao, J.; Kulinich, S.A.; Du, X. Tuning band structure of cadmium chalcogenide nanoflake arrays via alloying for efficient photoelectrochemical hydrogen evolution. *Langmuir* **2017**, *33*, 6457–6463. [CrossRef]

8. Zou, H.; Liu, M.; Zhou, D.; Zhang, X.; Liu, Y.; Yang, B.; Zhang, H. Employing CdSe$_x$Te$_{1-x}$ alloyed quantum dots to avoid the temperature-dependent emission shift of light-emitting diodes. *J. Phys. Chem. C* **2017**, *121*, 5313–5323. [CrossRef]

9. Hu, C.; Li, M.; Qiu, J.; Sun, Y.P. Design and fabrication of carbon dots for energy conversion and storage. *Chem. Soc. Rev.* **2019**, *48*, 2315–2337. [CrossRef]

10. Das, A.K.; Paria, S.; Maitra, A.; Halder, L.; Bera, A.; Bera, R.; Si, S.K.; De, A.; Ojha, S.; Bera, S.S.K.; et al. Highly rate capable nanoflower-like NiSe and WO$_3$@PPy composite electrode materials toward high energy density flexible all-solid-state asymmetric supercapacitor. *ACS Appl. Electron. Mater.* **2019**, *1*, 977–990. [CrossRef]

11. Das, A.; Deepa, M.; Ghosal, P. Dual function of molybdenum sulfide/C-cloth in enhancing the performance of fullerene nanosheets based solar cell and supercapacitor. *RSC Adv.* **2018**, *8*, 34984–34998. [CrossRef]

12. Zhu, S.; Li, Q.; Wei, Q.; Sun, R.; Liu, X.; An, Q.; Mai, L. NiSe2 Nanooctahedra as an anode material for high-rate and long-life sodium-ion battery. *ACS Appl. Mater. Interfaces* **2017**, *9*, 311–316. [CrossRef]

13. Kumar, P.N.; Narayanan, R.; Deepa, M.; Srivastava, A.K. Au@poly(acrylic acid) plasmons and C60 improve the light harvesting capability of a TiO2/CdS/CdSeS photoanode. *J. Mater. Chem. A* **2014**, *2*, 9771–9783. [CrossRef]

14. Pareek, A.; Paik, P.; Borse, P.H. Nanoniobia modification of CdS photoanode for an efficient and stable photoelectrochemical cell. *Langmuir* **2014**, *30*, 15540–15549. [CrossRef]

15. Vercelli, B.; Zotti, G.; Berlin, A. Alternate monolayers of CdSe nanocrystals and perylene tetracarboxylate: Quantum dot hypersensitization for dye-sensitized solar cells. *ACS Appl. Mater. Interfaces* **2012**, *4*, 3233–3238. [CrossRef]

16. Zhang, J.; Su, Y.; Zhu, Y.; Yun, J.; Yang, X. Photoelectrochemical biofuel cell with dendrimer-encapsulated CdSe nanoparticles-sensitized titanium dioxide as the photoanode. *New J. Chem.* **2014**, *38*, 2300–2304. [CrossRef]

17. Wang, J.; Lv, P.; Mu, Y.; Ding, D.; Liu, L.; Runa, A.; Feng, F.; Feng, S.; Fu, W.; Yang, H. A novel cage-like CdTe film with enhanced photoelectrochemical performance. *RSC Adv.* **2016**, *6*, 43489–43495. [CrossRef]

18. Kurnia, F.; Ng, Y.H.; Tang, Y.; Amal, R.; Valanoor, N.; Hart, J.N. ZnS thin films for visible-light active photoelectrodes: Effect of film morphology and crystal structure. *Cryst. Growth Des.* **2016**, *5*, 2461–2465. [CrossRef]

19. Kowalik, R.; Szaciłowski, K.; Żabiński, P. Photoelectrochemical study of ZnSe electrodeposition on Cu electrode. *J. Electroanal. Chem.* **2012**, *674*, 108–112. [CrossRef]

20. Jia, J.; Xue, P.; Hu, X.; Wang, Y.; Liu, E.; Fan, J. Electron-transfer cascade from CdSe@ZnSe core-shell quantum dot accelerates photoelectrochemical H$_2$ evolution on TiO$_2$ nanotube arrays. *J. Catal.* **2019**, *375*, 81–94. [CrossRef]

21. Bhagyaraj, S.; Perumbilavil, S.; Udayabashkar, R.; Mangalaraja, R.V.; Thomas, S.; Kalarikkal, N.; Oluwafemi, O.S.; Sreekanth, P.; Rednam, U.; Viswanathan, M.R. Tuning of nonlinear absorption in highly luminescent CdSe based quantum dots with core–shell and core/multi-shell architectures. *Phys. Chem. Chem. Phys.* **2019**, *21*, 11424–11434. [CrossRef] [PubMed]

22. Rosly, H.N.; Rahman, K.S.; Abdullah, S.F.; Harif, M.N.; Doroody, C.; Chelvanathan, P.; Misran, H.; Sopian, K.; Amin, N. The Role of Deposition Temperature in the Photovoltaic Properties of RF-Sputtered CdSe Thin Films. *Crystals* **2021**, *11*, 73. [CrossRef]

23. Amir, F.; Clark, K.; Maldonado, E.; Kirk, W.; Jiang, J.; Ager, J.; Yu, K.; Walukiewicz, W. Epitaxial growth of CdSexTe1−x thin films on Si(100) by molecular beam epitaxy using lattice mismatch graded structures. *J. Cryst. Growth* **2008**, *310*, 1081–1087. [CrossRef]

24. Matsumura, N.; Sakamoto, T.; Saraie, J. Growth conditions in molecular beam epitaxy for controlling CdSeTe epilayer composition. *J. Cryst. Growth* **2003**, *251*, 602–606. [CrossRef]

25. Noda, D.; Aoki, T.; Nakanishi, Y.; Hatanak, Y. Growth of CdZnTe and CdSeTe crystals for p–i–n radiation detectors. *J. Cryst. Growth* **2000**, *2*, 1121–1124. [CrossRef]

26. Wei, W.; Yang, Z.; Song, W.; Hu, F.; Luan, B.; Li, P.; Yin, H. Different CdSeTe structure determined photoelectrocatalytic reduction performance for carbon dioxide. *J. Colloid Interf. Sci.* **2017**, *496*, 327–333. [CrossRef] [PubMed]

27. Munshi, A.H.; Kephart, J.M.; Abbas, A.; Danielson, A.; Gélinas, G.; Beaudry, J.-N.; Barth, K.L.; Walls, J.M.; Sampath, W.S. Effect of CdCl$_2$ passivation treatment on microstructure and performance of CdSeTe/CdTe thin-film photovoltaic devices. *Sol. Energy Mater. Sol. C* **2018**, *186*, 256–259. [CrossRef]

28. Murali, K.R. Characteristics of slurry coated CdSeTe films. *Mater. Sci. Semicon. Proc.* **2010**, *13*, 193–198. [CrossRef]

29. Liu, G.; Ling, Z.; Wang, Y.; Zhao, H. Near-infrared CdSe$_x$Te$_{1-X}$@CdS "giant" quantum dots for efficient photoelectrochemical hydrogen generation. *Int. J. Hydrog. Energy* **2018**, *43*, 22064–22074. [CrossRef]

30. Hana, Z.; Chen, L.; Weng, Q.; Zhou, Y.; Wang, L.; Li, C.; Chen, J. Silica-coated gold nanorod@CdSeTe ternary quantum dots core/shell structure for fluorescence detection and dual-modal imaging. *Sens. Actuators B* **2018**, *258*, 508–516. [CrossRef]

31. Shinde, S.K.; Thombare, J.V.; Dubal, D.P.; Fulari, V.J. Electrochemical synthesis of photosensitive nano-nest like CdSe$_{0.6}$Te$_{0.4}$ thin films. *Appl. Surf. Sci.* **2013**, *282*, 561–565. [CrossRef]

32. Shinde, S.; Dubal, D.; Ghodake, G.; Fulari, V. Synthesis and characterization of chemically deposited flower-like CdSe0.6Te0.4 thin films for solar cell application. *Mater. Lett.* **2014**, *126*, 17–19. [CrossRef]

33. Shinde, S.K.; Ghodake, G.S.; Maile, N.C.; Dhaygude, H.D.; Kim, S.; Phule, A.D.; Patel, R.V.; Kim, D.Y. Porous CdSe$_{0.6}$Te$_{0.4}$ nanoflowers-nanosphere: Facile electrochemical synthesis and excellent for photoelectrochemical cell performance. *Ionics* **2017**, *23*, 2489–2496. [CrossRef]

34. Shinde, S.K.; Ghodake, G.S.; Dubal, D.P.; Dhaygude, H.D.; Kim, D.-Y.; Rath, M.C.; Fulari, V.J. Morphological modification of CdSe$_{0.6}$Te$_{0.4}$ nanostructures by electron irradiation and the effect on photoelectrochemical cells. *J. Mater. Sci.-Mater. Electron.* **2017**, *28*, 1976–1984. [CrossRef]

35. Shinde, S.K.; Ghodake, G.S.; Dubal, D.P.; Lohar, G.M.; Lee, D.S.; Fulari, V.J. Structural, optical, and photo-electrochemical properties of marygold-like CdSe$_{0.6}$Te$_{0.4}$ synthesized by electrochemical route. *Ceram. Int.* **2014**, *40*, 11519–11524. [CrossRef]

36. Shinde, S.K.; Dubal, D.P.; Ghodake, G.S.; Fulari, V.J. Electronic impurities (Fe, Mn) doping in CdSe nanostructures for improvements in photoelectrochemical applications. *RSC Adv.* **2014**, *4*, 33184–33189. [CrossRef]

37. Shinde, S.K.; Dubal, D.P.; Ghodake, G.S.; Lee, D.S.; Lohar, G.M.; Rath, M.C.; Fulari, V.J. Materials Baking impact of Fe composition on CdSe films for solar cell application. *Mater. Lett.* **2014**, *132*, 243–246. [CrossRef]

38. Ghodake, V.J.; Fulari, D.-Y.; Kim, D.Y. High electrochemical performance of nanoflakes like CuO electrode by successive ionic layer adsorption and reaction (SILAR) method. *J. Ind. Eng. Chem.* **2017**, *52*, 12–17.

39. Shinde, S.; Jalak, M.; Ghodake, G.; Maile, N.; Yadav, H.; Jagadale, A.; Shahzad, A.; Lee, D.; Kadam, A.; Fulari, V.; et al. Flower-like NiCo2O4/NiCo2S4 electrodes on Ni mesh for higher supercapacitor applications. *Ceram. Int.* **2019**, *45*, 17192–17203. [CrossRef]

40. Dhaygude, H.D.; Shinde, S.K.; Takale, M.V.; Dubal, D.P.; Lohar, G.M.; Fulari, V.J. Electrodeposited nanosphere like CdxZn12xS electrodes for photoelectrochemical cell. *J. Mater. Sci. Mater. Electron.* **2016**, *27*, 5145–5152. [CrossRef]

41. MacDonald, B.I.; Martucci, A.; Rubanov, S.; Watkins, S.E.; Mulvaney, P.; Jasieniak, J.J. Layer-by-layer assembly of sintered CdSexTe1−X nanocrystal solar Cells. *ACS Nano* **2012**, *6*, 5995–6004. [CrossRef]

42. Marcos, L.V.R. –D.; Kalaiselvi, S.M.P.; Leong, O.B.; Das, P.K.; Breese, M.B.H.; Rusydio, A. Optical constants and absorption properties of Te and TeO thin films in the 13-14 nm spectral range. *Opt. Express* **2020**, *28*, 12922–12935. [CrossRef] [PubMed]

43. Shinde, S.K.; Ghodake, G.S.; Dubal, D.P.; Dhaygude, H.D.; Kim, D.-Y.; Fulari, V.J. Enhanced photoelectrochemical properties of nanoflower-like hexagonal CdSe0.6Te0.4: Effect of electron beam irradiation. *J. Ind. Eng. Chem.* **2017**, *45*, 92–98. [CrossRef]

44. Xue, J.; Chen, X.; Liu, S.; Zheng, F.; He, L.; Li, L.; Zhu, J.-J. Highly Enhanced Fluorescence of CdSeTe Quantum Dots Coated with Polyanilines via In-Situ Polymerization and Cell Imaging Application. *ACS Appl. Mater. Interfaces* **2015**, *7*, 19126–19133. [CrossRef]

45. Li, Z.-J.; Fan, X.-B.; Li, X.-B.; Li, J.-X.; Zhan, F.; Tao, Y.; Zhang, X.; Kong, Q.-Y.; Zhao, N.-J.; Zhang, J.-P.; et al. Direct synthesis of all-inorganic heterostructured CdSe/CdS QDs in aqueous solution for improved photocatalytic hydrogen generation. *J. Mater. Chem. A* **2017**, *5*, 10365–10373. [CrossRef]

46. Yuan, Y.-J.; Chen, D.; Yu, Z.-T.; Zou, Z.-G. Cadmium sulfide-based nanomaterials for photocatalytic hydrogen production. *J. Mater. Chem. A* **2018**, *6*, 11606–11630. [CrossRef]

47. Dhaygude, H.; Shinde, S.; Takale, M.; Lohar, G.; Rath, M.; Fulari, V. Effect of electron irradiation on structural, morphological and photoluminescence properties of ZnS thin films. *Ceram. Int.* **2016**, *42*, 10159–10164. [CrossRef]

48. Dhaygude, H.D.; Shinde, S.K.; Dubal, D.P.; Rath, M.C.; Fulari, V.J. Effect of electron beam irradiation on electro synthesized hexagonal Cd$_{0.3}$Zn$_{0.7}$S nanosphere with excellent application in solar cell. *Appl. Surf. Sci.* **2016**, *368*, 1–7. [CrossRef]

49. Shinde, S.K.; Ghodake, G.S.; Velhal, N.B.; Takale, M.V.; Kim, D.-Y.; Rath, M.C.; Dhaygude, H.D.; Fulari, V.J. Enhanced solar cell performance of electron beam irradiated CdS photoanode by electrodeposition method. *J. Solid State Electr.* **2017**, *21*, 1517–1522. [CrossRef]

50. Shinde, S.K.; Kim, D.-Y.; Lee, D.S.; Ghodake, G.S.; Kadam, A.N.; Fulari, A.V.; Nawaz, M.; Shahzad, A.; Rath, M.C.; Fulari, V.J. Effect of electron beam irradiation on chemically synthesized nanoflake-like CdS electrodes for photoelectrochemical applications. *Colloids Surf. B* **2018**, *164*, 255–261. [CrossRef] [PubMed]

51. Pan, A.; Yang, H.; Liu, R.; Yu, R.; Zou, B.; Wang, Z. Color-tunable photoluminescence of alloyed CdS$_x$Se$_{1−X}$ nanobelts. *J. Am. Chem. Soc.* **2005**, *127*, 15692–15693. [CrossRef]

52. Pan, J.; Utama, M.I.B.; Zhang, Q.; Liu, X.; Peng, B.; Wong, L.M.; Sum, T.C.; Wang, S.; Xion, Q. Composition-tunable vertically aligned CdS$_x$Se$_{1−X}$ nanowire arrays via van der waals epitaxy: Investigation of optical properties and photocatalytic behavior. *Adv. Mater.* **2012**, *24*, 4151–4156. [CrossRef]

53. Muthukumarasamy, N.; Balasundaraprabhu, R.; Jayakumar, S.; Kannan, M.D.; Ramanathaswamy, P. Compositional dependence of optical properties of hot wall deposited CdSe$_x$Te$_{1−X}$ thin films. *Phys. Stat. Sol.* **2004**, *201*, 2312–2318. [CrossRef]

54. Velumani, S.; Mathew, X.; Sebastian, P.J. Structural and optical characterization of hot wall deposited CdSe$_x$Te$_{1−x}$ films. *Sol. Energ. Mater. Sol. C* **2003**, *76*, 359–368. [CrossRef]

55. Sathyamoorthy, R.; Sudhagar, P.; Kumar, R.S.; Matheswaran, P.; Nair, R.G. Facile synthesis of thiol-stabilized CdSe$_x$Te$_{1−x}$ nanocrystals. *Phys. B* **2011**, *406*, 715–719. [CrossRef]